

RESEARCH

Open Access



# Synergistic antibacterial activity of chitosan-polyethylene glycol nanocomposites films containing ZIF-8 and doxycycline

Fahimeh Jamiri<sup>1</sup>, Bahar Nayeri Fasaeei<sup>1\*</sup> , Seyed Mehdi Joghataei<sup>1</sup> , Ramak Yahyaraeyat<sup>1</sup> and Azin Mazloom-Jalali<sup>2</sup>

## Abstract

**Background** Antibiotic resistance is a growing global threat due to antibiotic overuse and limited treatment options. Multidrug-resistant bacteria, like *Staphylococcus aureus* and *Escherichia coli*, increase infection complexity and mortality. This study explores nanocomposite films of ZIF-8 nanoparticles and Doxycycline (Dox) to enhance antibacterial efficacy. In this study, nanocomposite films composed of chitosan (CS) and polyethylene glycol (PEG), incorporating zeolitic imidazolate framework-8 (ZIF-8) nanoparticles and DOX, were developed. These films were characterized by their morphological, mechanical, antibacterial, and drug-release properties. Antibacterial efficacy was evaluated using disk diffusion, broth microdilution, and checkerboard assay methods to determine MICs and potential synergistic effects.

**Results** The nanocomposite films demonstrated flexibility, semi-transparency, and a yellowish-brown hue, with films containing ZIF-8 nanoparticles being thicker ( $79 \pm 0.2 \mu\text{m}$ ) than those without ( $54 \pm 0.5 \mu\text{m}$ ). The tensile strength was enhanced with the incorporation of ZIF-8, peaking at 53.12 MPa for the CS-PEG-G-10% DOX-4% ZIF-8 film. XRD analysis confirmed the crystallinity of the ZIF-8 and DOX, with distinct peaks observed for each material. The drug release studies revealed an initial burst followed by sustained release, with higher release rates in acidic environments compared to neutral and alkaline media. The CS-PEG-G-10% DOX-4% ZIF-8 nanocomposite film demonstrated significantly higher antibacterial activity, achieving the lowest MIC values, particularly against *S. aureus* (22.5 mm inhibition zone) compared to *E. coli* (14 mm inhibition zone). Additionally, a notable synergistic effect was observed between CS-PEG-G-10% DOX and CS-PEG-G-10% DOX, with FICI values below 0.5.

**Conclusions** The CS-PEG-G-10% DOX-4% ZIF-8 nanocomposite exhibits enhanced antibacterial efficacy and optimal properties, positioning it as a strong candidate for developing effective treatments against multidrug-resistant pathogens.

**Keywords** Doxycycline, ZIF-8 nanoparticle, Nanocomposites, Antibacterial drugs, *Staphylococcus aureus*, *Escherichia coli*, Metal-organic frameworks, Chitosan, Drug delivery

\*Correspondence:

Bahar Nayeri Fasaeei  
nayerib@ut.ac.ir

<sup>1</sup>Department of Microbiology and Immunology, Faculty of Veterinary Medicine, University of Tehran, Tehran, Iran

<sup>2</sup>Department of Chemistry, Amir Kabir University of Technology (Tehran Polytechnic), P.O.Box: 15875-4413, Tehran, Iran



© The Author(s) 2025. **Open Access** This article is licensed under a Creative Commons Attribution-NonCommercial-NoDerivatives 4.0 International License, which permits any non-commercial use, sharing, distribution and reproduction in any medium or format, as long as you give appropriate credit to the original author(s) and the source, provide a link to the Creative Commons licence, and indicate if you modified the licensed material. You do not have permission under this licence to share adapted material derived from this article or parts of it. The images or other third party material in this article are included in the article's Creative Commons licence, unless indicated otherwise in a credit line to the material. If material is not included in the article's Creative Commons licence and your intended use is not permitted by statutory regulation or exceeds the permitted use, you will need to obtain permission directly from the copyright holder. To view a copy of this licence, visit <http://creativecommons.org/licenses/by-nc-nd/4.0/>.

## Introduction

The emergence of resistant bacteria poses a significant global threat, primarily due to the widespread misuse of antibiotics and the scarcity of new antibacterial drugs. This issue is further exacerbated by the continuous appearance of bacterial isolates resistant to multiple antibiotics, greatly reducing their effectiveness in treating infections [1]. Bacterial isolates resistant to two distinct classes of antibiotics are classified as multidrug-resistant (MDR) bacteria. Infections caused by MDR bacteria are associated with a significantly higher mortality risk than those caused by non-MDR bacteria [2, 3].

*Staphylococcus aureus*, a Gram-positive bacterial pathogen, is a major cause of severe infections, particularly with the rise of methicillin-resistant *S. aureus* (MRSA), which is resistant to many antibiotics. MRSA is a notorious cause of hospital-acquired infections and is linked to significant morbidity and mortality [4, 5]. Similarly, Gram-negative bacteria like *Escherichia coli* have become prominent MDR pathogens due to the limited availability of effective antibiotics against them [3].

Currently, significant efforts are directed towards developing innovative formulations by combining new biomaterial-derived excipients with existing antibacterial drugs to enhance safety, efficacy, and cost-effectiveness in both production and disposal [6–10]. Chitosan (CS), a natural biopolymer, has gained widespread use in drug delivery due to its biocompatibility, biodegradability, low cost, and abundance of amine and hydroxyl groups. It also exhibits nontoxicity, antibacterial properties, and hemostatic capabilities [11–13]. Additionally, as a cationic biopolymer containing amino groups, CS can interact with the anionic components of microbial cell membranes, leading to membrane disruption and the leakage of intracellular contents [14]. Metal-organic frameworks (MOFs) represent an emerging class of porous materials made from inorganic metal ions connected by organic linkers [15, 16], among various metals used to synthesize MOFs, those containing zinc and iron show promise for clinical applications, including drug delivery. These outstanding properties are attributed to characteristics such as high biodegradability, biocompatibility, pH-sensitive dissolution, a broad range of pore sizes, significant porosity, a large surface area, thermal stability, and diverse chemical composition [17, 18].

Over the past decades, controlled drug delivery technology has advanced significantly, allowing therapeutic drugs to be delivered at a predetermined rate, either locally or systemically, over a specified period to achieve desired effects safely [19, 20]. Significant advancements have been made in developing drug delivery systems that offer improved efficacy, safety, bioavailability, controlled release, and prolonged therapeutic effects [10]. Drug release from pharmaceutical systems can be regulated

through various mechanisms that involve their physicochemical properties. One strategy for controlling drug release is the incorporation of a drug into a substrate with specific biological, chemical, and mechanical properties [21]. Zeolitic imidazolate framework-8 (ZIF-8), a subclass of MOFs composed of zinc ions and 2-methylimidazole ligands, has shown chemical stability in aqueous and basic media and reported surface areas of up to approximately 1800 m<sup>2</sup>/g [21, 22]. ZIF-8 nanoparticles have been successfully used for the controlled release of the 6-mercaptopurine drug against cancer cells [23]. Additionally, Another study highlights the antibacterial properties of ZIF-8 nanoparticles, revealing increased effectiveness against gram-positive bacteria when paired with Vancomycin, along with significant photoinactivation capabilities under light exposure [24]. Another investigation on ZIF-8 emphasizes its antibacterial properties, showing its effectiveness in inhibiting the growth of *Staphylococcus aureus* and *Pseudomonas aeruginosa* when used in combination with the antibiotic Ciprofloxacin [25]. The synthesis and coating of ZIF-8 with sodium alginate were explored as a green and bioactive platform for the controlled release of Metformin [26]. Additionally, the natural Physcion was encapsulated within ZIF-8 and examined for its antimicrobial potential through the release of the encapsulated drug [27].

Doxycycline (Dox), a semi-synthetic antimicrobial drug derived from oxytetracycline, has been widely used since 1967 to treat a broad spectrum of bacterial infections. Its versatility extends to antiviral, antiparasitic, anticancer, neuroprotective, anti-inflammatory, and wound-healing applications [28]. Dox may benefit from COVID-19 treatment due to its antiviral and anti-inflammatory properties, which help mitigate the cytokine storm and prevent lung damage [29]. Despite its extensive therapeutic potential, Dox faces challenges such as instability in physiological environments, poor cellular penetration, and adverse gastrointestinal effects. Additionally, bacteria can develop resistance to Dox, complicating its efficacy. Pharmaceutical nanotechnology offers a promising solution to these limitations by enhancing drug delivery, targeting specific tissues, organs, or cells, reducing dosage requirements, and minimizing side effects [30, 31].

Nanostructured Drug Delivery Systems (NDDS) are designed to protect their cargo and ensure excellent cellular penetration [32]. Positively charged nanostructures, for example, enhance electrostatic interactions with negatively charged bacterial walls, improving the bactericidal action of antibiotics. Moreover, nano structuration can prevent microbial resistance against specific drug classes, making Dox-loaded NDDS a potent alternative for boosting efficacy. Standard nanoparticle matrices for drug delivery include polymeric, lipid, and inorganic materials, with the choice depending on the drug's physicochemical

properties and intended application. Studies have shown an increasing trend in the use of Dox-loaded nanoparticles, peaking in 2020, highlighting the growing interest in this drug and its nanotechnological delivery platforms [30, 33].

The current study investigates the antibacterial properties of ZIF-8 nanoparticles and Dox, explicitly targeting the challenge of antibiotic resistance. The application of nanotechnology and nanocomposites is pivotal, as it enhances the effectiveness of the mentioned compounds, reduces the required dosage, and helps prevent the development of drug resistance. By evaluating the antibacterial effects of nanocomposite films made of ZIF-8 and Dox against *E. coli* and *S. aureus*—known for their resistance to various antibiotics—this research aims to uncover innovative strategies to combat bacterial infections. Enhancing the antibacterial properties of ZIF-8 and DOX through nanocomposite films could significantly lower the necessary drug dosage, thereby minimizing potential side effects and toxicity, ultimately improving outcomes.

## Materials and methods

### Materials

High molecular weight CS, with a deacetylation degree of at least 75% and a viscosity range of 200–800 cps, along with polyethylene glycol (PEG) with an average molecular weight of 400,000, were procured from Sigma–Aldrich. Additional reagents, including zinc nitrate hexahydrate ( $\text{Zn}(\text{NO}_3)_2 \cdot 6 \text{H}_2\text{O}$ ), 2-methylimidazole, and 3-(4,5-dimethylthiazole-2-yl)-2,5-diphenyltetrazolium bromide (MTT), were also sourced from Sigma–Aldrich. Other chemicals, such as methanol, acetic acid, sodium chloride (NaCl), potassium chloride (KCl), sodium hydroxide (NaOH), hydrochloric acid (HCl), potassium dihydrogen phosphate ( $\text{KH}_2\text{PO}_4$ ), disodium hydrogen phosphate ( $\text{Na}_2\text{HPO}_4$ ), and glycerin (G) were obtained from Merck, Germany. The antibiotic DOX (Hyclate) 500 was provided by Pars Dopharma Pharmaceutical Company, Tehran, Iran. All materials were used as supplied without any additional purification. Commercial antibiotic discs of DOX (30  $\mu\text{g}$ ) and Gentamicin (30  $\mu\text{g}$ ) were sourced from Thermo Fisher Scientific Inc., USA. Blank paper discs were procured from Padtan-Teb Company, Iran, and all culture media were obtained from Merck. Distilled water was utilized in all experiments to maintain purity and consistency in the preparation of solutions and formulations.

### Synthesis of ZIF-8 nanoparticles

ZIF-8 nanocrystals were synthesized using the precipitation method as described in prior studies [34, 35]. Initially, a solution of  $\text{Zn}(\text{NO}_3)_2 \cdot 6 \text{H}_2\text{O}$  (2 mmol) in methanol was added to a methanolic solution of 2-methylimidazole (16 mmol) while stirring continuously. The

mixture gradually became turbid, indicating the formation of nanocrystals. After 1 h, the resulting milky dispersion was subjected to centrifugation to collect the nanocrystals. The collected nanocrystals were then washed with fresh methanol and dried at 40 °C in air. The synthesis resulted in a yield of approximately 50%, based on zinc<sup>2+</sup> nitrate hexahydrate.

### Fabrication of nanocomposite films

Nanocomposite films were fabricated using techniques such as solution casting, ultrasonic-assisted mixing, and nanoparticle dispersion [34, 36]. A solution of CS and PEG was created in a 5% aqueous acetic acid solution by subjecting the mixture to sonication for 30 min, maintaining a weight ratio of 70:30 for CS to PEG. Glycerin (G) was then added to this mixture at 5 wt% relative to the total weight of the CS and PEG polymers, serving as a plasticizer. Next, DOX was introduced into the polymer solution at a concentration of 10 wt% based on the total weight of CS-PEG. In the subsequent stage, ZIF-8 nanoparticles were added to the CS-PEG-G-DOX solution at a concentration of 4 wt% relative to the CS-PEG polymers. A control solution was also prepared without the addition of nanoparticles. All mixtures were subjected to ultrasonication for 1 h to ensure homogeneous dispersion of ZIF-8 and DOX nanoparticles. Afterward, the nanoparticle suspensions were continuously stirred for 24 h to ensure even dispersion.

For the preparation of the final nanocomposite films, the homogeneous mixtures were poured into plates and placed in a furnace at 50 °C for 12 h to allow for solvent evaporation and the formation of the desired films. The resulting films included CS-PEG-G, CS-PEG-G-4% ZIF-8, CS-PEG-G-10% DOX, and CS-PEG-G-10% DOX-4% ZIF-8.

### Characteristics of nanocomposite films

To examine the morphology and size of the CS-PEG-G-10% DOX-4% ZIF-8 nanocomposite film and ZIF-8 Nanoparticles, scanning electron microscopy (SEM) was conducted using a Philips XL30 instrument. The samples were gold-coated and analyzed under vacuum at an acceleration voltage of 20 kV. X-ray diffraction (XRD) patterns of the films were recorded using an INEL EQUINOX 3000 X-ray diffractometer. The measurements were taken in the range of  $2\theta = 2\text{--}120^\circ$  with Cu-K $\alpha$  radiation (wavelength = 1.537472 Å), operating at 40 kV and 30 mA with a scan rate of 2°/min. The d-spacing values were calculated using Bragg's equation,  $n\lambda = 2d\sin\theta$ , where  $\lambda = 15.41874$  nm and  $\theta$  stands for the diffraction angle (in degree) assigned to the peak with the highest intensity. The tensile strength of the films was evaluated using an Instron 5566 Universal Testing Machine (UTM) at a crosshead speed of 1 mm/min. The release

profile of DOX from the CS-PEG-G-10% DOX-4% ZIF-8 and CS-PEG-G-10% DOX was analyzed using a UV-visible spectrophotometer (Perkin Elmer). Each film sample, weighing 30 mg, was immersed in 8 mL of various media (acidic pH=4.2, PBS solution at pH=7.4, and alkaline pH=12.5) and incubated at 25 °C for 100 h with shaking. To monitor the cumulative release of DOX, 1 mL of the solution was withdrawn at predetermined intervals and replaced with an equal volume of fresh medium. The absorbance of the collected samples was measured at approximately 194 and 261 nm to determine the amount of DOX released over time [34, 36].

### Microorganisms

The antibacterial activity of the ordered nanocomposites was evaluated using two bacterial strains: *S. aureus* ATCC<sup>®</sup> 29,213<sup>™</sup>, a Gram-positive bacterium, and *E. coli* ATCC<sup>®</sup> 35,218<sup>™</sup>, a Gram-negative bacterium. Lyophilized cultures were obtained from Liofilchem (Roseto Degli Abruzzi, Italy). All bacterial strains were preserved at -70 °C and sub-cultured on blood agar at 37 °C overnight before the assay.

### In vitro antibacterial activities

The antibacterial activity of nanocomposite films was evaluated against the mentioned bacterial strains. Mueller Hinton Broth (MHB) and Mueller Hinton Agar (MHA) were used as test media following standard procedures, as described below. The thickness of the agar medium was kept equal in all Petri dishes. All experiments were conducted in triplicate.

### Disk diffusion

The antibacterial activity of nanocomposite films was evaluated using a disc diffusion method adapted from the Clinical and Laboratory Standards Institute (CLSI) standard [37]. A standardized inoculum of  $1.5 \times 10^6$  CFU/mL was prepared by suspending three colonies from an overnight culture at 37 °C on MHA into 5 mL of sterile 0.85% NaCl solution, followed by a 1:100 dilution with MHB. Then, 100 µL of the standardized inoculum was spread across the surface of MHA Petri dishes. 0.004 g of each nanocomposite film was cut into 3 mm x 3 mm pieces and sterilized using 70% alcohol. Subsequently, they were carefully placed onto MHA Petri dishes that had been pre-inoculated and air-dried to eliminate surface moisture. To measure the film extract, which was prepared in PBS under sterile conditions, 10 µL of nanocomposite film extracts were separately applied to blank paper discs. These discs facilitated the release of antibacterial substances into the culture medium containing the targeted bacteria. They were then gently placed on MHA Petri dishes previously inoculated with 100 µL of the standard bacterial inoculum. A blank disc served as the negative

control. After placing the specific nanocomposite films and discs at each stage, the Petri dishes were incubated at  $37 \pm 1$  °C for 24 h. After incubation, the inhibition zone diameters were measured. For each sample, the average of three measurements was calculated.

### Assessing strain sensitivity to DOX

Based on the guidelines of CLSI M02, the sensitivity of bacterial strains to DOX (30 µg) commercial antibiotic disks was investigated by disk diffusion method [37].

### Broth microdilution

The antibacterial activity was assessed using the broth microdilution method, following adapted CLSI guidelines [38], to determine the minimum inhibitory concentration (MIC) and minimum bactericidal concentration (MBC). In this procedure, film extracts were prepared in PBS under sterile conditions.

Volumes of 130 µL of fresh MHB and 20 µL of bacterial inoculation with a concentration of  $1.5 \times 10^6$  CFU/mL during the logarithmic growth phase were added to the wells of sterile 96-well microplates. Then, 20 µL of successive dilutions of the nanocomposite film extracts (It began at a concentration of 3 mg/ml) were added to each designated well. Gentamicin at the same concentration range was used as the positive control, while a culture medium without any antibacterial agent served as the negative control. After 24 h of incubation at 35 °C, cell growth in each well was assessed by measuring the optical density with a microplate reader (Thermo, Madison, WI, USA). The MIC was defined as the lowest concentration of nanocomposite film extracts at which no apparent growth (turbidity) was observed, measured by OD at 600 nm. The assays were conducted in triplicate, and the MIC for each antimicrobial material was determined in at least three experiments. Additionally, 0.02 mL from each well was inoculated onto nutrient agar plates to determine the MBC. The MBC was considered the lowest concentration, with no colonies observed on the plates after incubation.

### Checkerboard assay

The checkerboard technique was employed to evaluate the synergistic effect of CS-PEG-G-4% ZIF-8 and CS-PEG-G-10% DOX against *S. aureus* and *E. coli* following established methods [39, 40]. These strains were cultured overnight in tryptic soy broth (TSB) at 37 °C to achieve the desired growth phase for further testing.

The Checkerboard Assay was conducted in 96-well microtiter plates. Each well in the plate contained a total volume of 100 µL, consisting of 50 µL of one antimicrobial agent (CS-PEG-G-4% ZIF-8 or CS-PEG-G-10% DOX) with two-fold serial dilutions of the nanocomposite film extracts. These dilutions covered a wide range

of concentrations, starting from the MIC of each agent. Additionally, 50  $\mu$ l of bacterial suspension, adjusted to  $1 \times 10^6$  CFU/ml, was added to each well. In the assay, the first row of wells contained decreasing concentrations of CS-PEG-G-4% ZIF-8 or CS-PEG-G-10% DOX, while the first column contained decreasing concentrations of the second antimicrobial agent. Each well, therefore contained a combination of varying concentrations of the two agents, allowing for different ratios to be tested against the bacterial strains. The positive control consisted of wells containing only bacterial suspension without any antimicrobial agents, while the negative control included wells with antimicrobial agents but no bacterial inoculation. The plates were incubated at 37 °C for 24 h to allow for bacterial growth and interaction with the antimicrobial agents. Afterward, the effects were assessed based on growth inhibition, indicating potential synergistic, additive, or antagonistic interactions.

After incubation, the MIC was determined by visual inspection and confirmed via optical density at 600 nm using a microplate reader. The fractional inhibitory concentration index (FICI) was calculated to assess the nature of the interaction between CS-PEG-G-4% ZIF-8 and CS-PEG-G-10% DOX. The FICI for each combination was calculated as follows:  $FICI = (\text{MIC of CS-PEG-G-4\% ZIF-8 in combination} / \text{MIC of CS-PEG-G-4\% ZIF-8 alone}) + (\text{MIC of CS-PEG-G-10\% DOX in combination} / \text{MIC of CS-PEG-G-10\% DOX alone})$ . FICI values were interpreted as synergistic ( $\leq 0.5$ ), additive ( $0.5 < FICI \leq 1$ ), indifferent ( $1 < FICI \leq 4$ ), or antagonistic ( $> 4$ ), providing insights into the potential enhancement of antibacterial activity when the two nanocomposites were used in combination.

### Statistical analysis

Statistical analysis was performed using GraphPad Prism 10.3.1 software. All experiments were conducted in triplicate, and the data were presented as mean  $\pm$  standard deviation. The differences between the means of the experimental groups were evaluated using ANOVA followed by Tukey's post-hoc test for multiple comparisons. A p-value of less than 0.05 was considered statistically significant. Additionally, the FICI values were calculated, and their interactions (synergy, additive, indifferent, or antagonistic effects) were categorized accordingly [2, 41, 42].

## Results

### Results of nanocomposite film characteristics

Regarding the physical properties, the nanocomposite films produced were flexible, semi-transparent, and had a yellowish-brown color. The thickness of the layers containing ZIF-8 nanoparticles was approximately  $79 \pm 0.2$   $\mu$ m, whereas the films without ZIF-8

nanoparticles (CS-PEG-G-10% DOX and CS-PEG-G) had a thickness of  $54 \pm 0.5$   $\mu$ m. Additionally, the tensile strength (MPa) was 32.46 for the CS-PEG-G film, 50.68 for the CS-PEG-G-4% ZIF-8 film, 33.16 for the CS-PEG-G-10% DOX film, and 53.12 for the CS-PEG-G-10% DOX-4% ZIF-8 film. The SEM micrographs of ZIF-8 nanoparticles, as well as CS-PEG-G film comprising ZIF-8 nanoparticles and DOX, are presented in Fig. 1. The ZIF-8 nanoparticles appear to be nearly spherical with an average size of 80 nm, showing signs of agglomeration structure composed of clusters of nanoscale particles, making it challenging to identify individual particles (Fig. 1-e). The micrograph shows spherical and cauliflower-like morphologies, characteristic of ZIF-8 crystalline formation. The SEM micrographs of the CS-PEG-G-10% DOX-4% ZIF-8 film exhibit a heterogeneous surface morphology featuring needle-like and rod-shaped crystalline structures. The needle-like ZIF-8 crystals have an average length ranging from approximately 1 to 5  $\mu$ m. The surface is interspersed with smaller granular particles, likely indicating the presence of DOX, with particle sizes generally below 500 nm. In the micrograph at 10,000x magnification, the larger clusters of needle-like structures are more visible, with individual clusters spanning areas of approximately 10 to 20  $\mu$ m in diameter. The lower magnification images show a uniform distribution of these crystalline and granular structures across the surface, suggesting a consistent morphology throughout the film.

The XRD analysis of CS revealed two peaks at 20.47° (with 25% intensity) and 23.93° (with 100% intensity), indicating the presence of inter- and intramolecular hydrogen bonding between its amino and hydroxyl groups. This pattern aligns with those reported in the literature, confirming the sample's purity [43]. The low-angle XRD pattern of ZIF-8 nanoparticles displayed sharp characteristic peaks at 4.28° (with 100% intensity), 9.43°, 15.7°, and 19.4°, consistent with the ZIF-8 structure. These observations confirmed the high crystallinity and successful synthesis of the ZIF-8 particles, as the presence of these sharp peaks without any additional signals indicates the formation of a pure phase [34, 44]. The XRD pattern for PEG powder showed a crystalline structure with two sharp peaks at 9.39° (100% intensity) and 14.52°, along with weaker peaks at around 22.31°, 26.45°, 35.64°, 39.00°, 44.23°, and 46.71°. The DOX drug exhibits a pattern of sharp peaks, indicating its high crystallinity, with notable peaks at  $2\theta = 4.35^\circ$  (100% intensity) and 7.25°. For the CS-PEG-G-10% DOX film, the XRD pattern exhibited a broad peak centered at 31.42°, attributed to the combined presence of CS, PEG, and the drug DOX. The XRD patterns of the two nanocomposite films with ZIF-8 nanoparticles display broad peaks, with a peak centered at 23.06° for CS-PEG-G-4% ZIF-8 and another

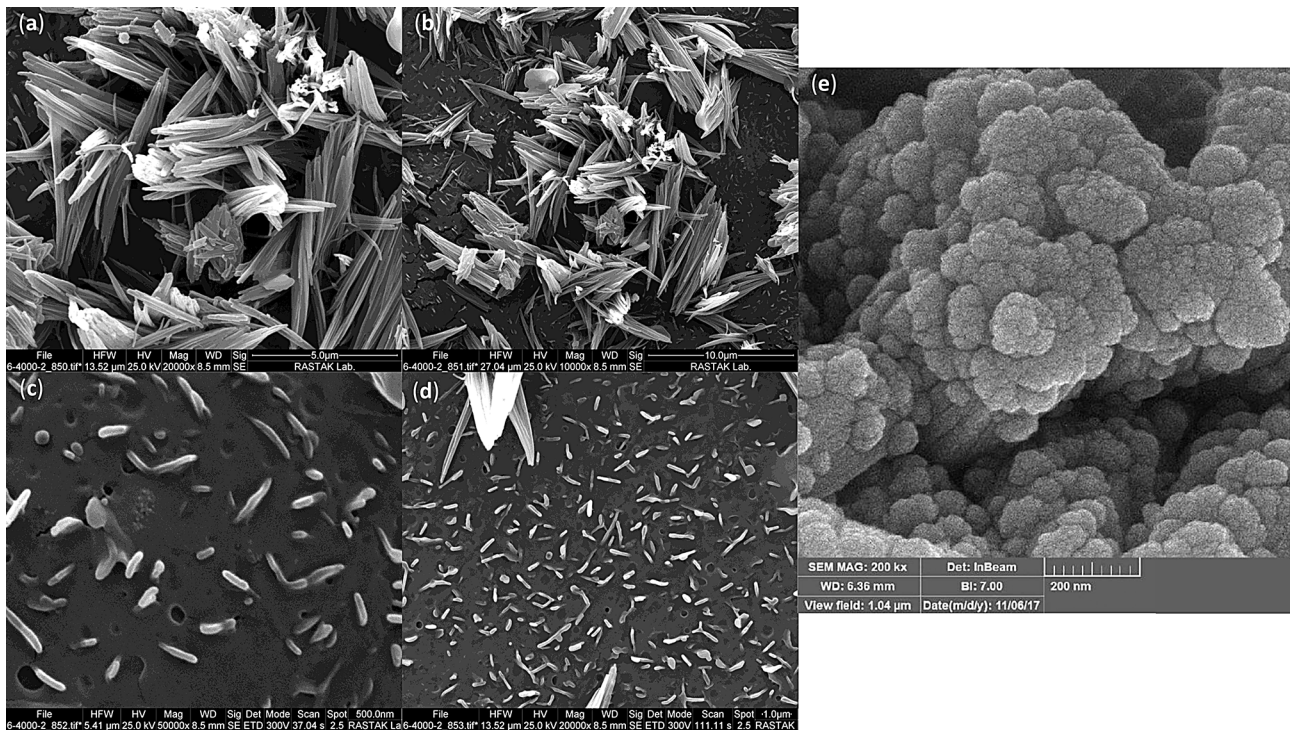


**Fig. 1** SEM images showing the morphology and surface characteristics of the nanocomposite films. (a) and (b) depict the overall structure and distribution of ZIF-8 nanoparticles within the polymer matrix, revealing a crystalline and layered morphology at magnifications of 20,000x and 10,000x, respectively. (c) illustrates a higher magnification (50,000x) view of the film, highlighting the dispersed nanoparticle clusters and their integration with the polymer matrix. (d) provides an even closer look at the surface morphology at 20,000x, displaying a more uniform dispersion of ZIF-8 particles. (e) focuses on the detailed morphology of individual ZIF-8 nanoparticles, showing their almost spherical shape and tendency to form agglomerates, with an average size around 80 nm at a magnification of 200,000x

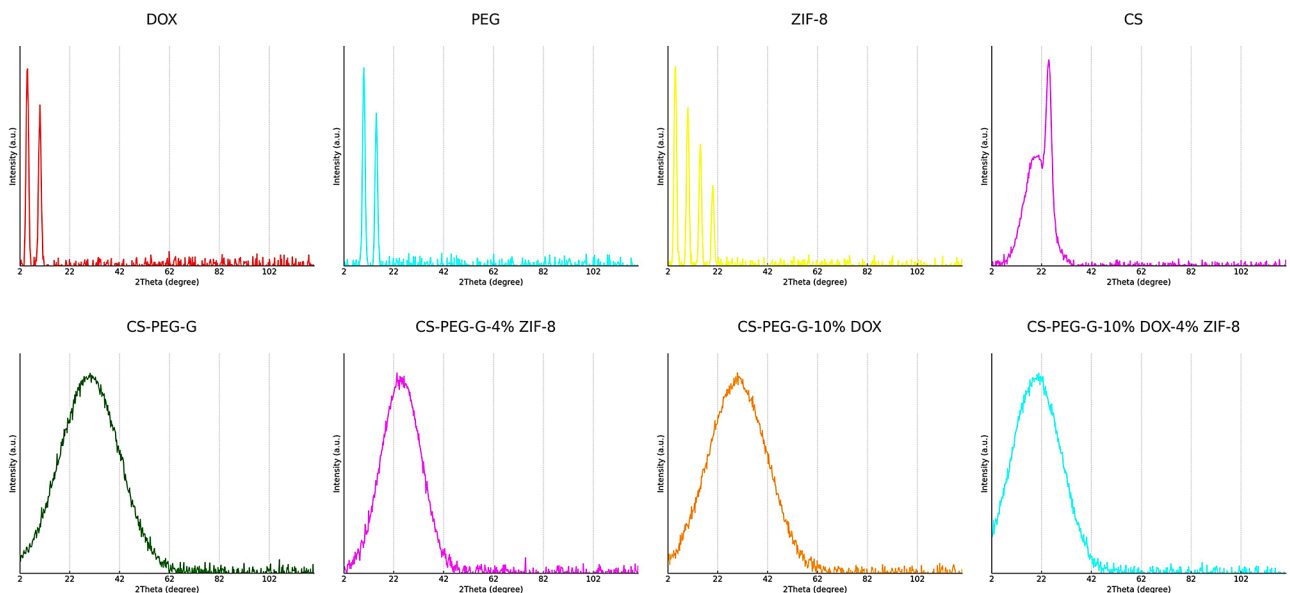


**Fig. 2** XRD patterns of CS, PEG, DOX, ZIF-8, and their nanocomposite films

at  $21.12^\circ$  for CS-PEG-G-10% DOX-4% ZIF-8, as shown in the figure. The CS-PEG-G film exhibited a pattern similar to that of the CS-PEG-G-10% DOX film, both featuring broad peaks centered around  $2\theta = 32^\circ$  (Fig. 2).

The d-spacing values for CS, PEG, and DOX are 44.56, 37.56, and 123.90 nm, respectively. Based on the center of the peaks with the highest intensity in the films, the inter-chain distances were calculated as follows:

38.76 nm for CS-PEG-G, 39.23 nm for CS-PEG-G-10% DOX, 43.62 nm for CS-PEG-G-4% ZIF-8, and 44.12 nm for CS-PEG-G-10% DOX-4% ZIF-8.

During the UV–Vis analysis, the release of DOX from the CS-PEG-G-10% DOX-4% ZIF-8 and CS-PEG-G-10% DOX nanocomposite films was evaluated over 24 h for films in acidic solution and over 100 h for those in neutral and alkaline media, as shown in Fig. 3. An initial burst release of the drug was observed within approximately 3 h in acidic media, 8 h in neutral media, and 10 h in alkaline media. Following this rapid release, the DOX was gradually released over time, indicating a sustained release phase. As illustrated in Fig. 3, films immersed in PBS (pH 7.4) and alkaline media demonstrated slower release rates compared to those in an acidic solution. In neutral and alkaline conditions, about 40% of the drug

was released quickly, followed by a more controlled release over the following days. In contrast, the drug release in acidic conditions reached 65% within the first 4.5 h. Notably, in the acidic environment, the film without nanoparticles showed the highest release rate. It is important to note that CS-PEG-G-10% DOX, which lacked ZIF-8 nanoparticles, exhibited a higher release rate compared to CS-PEG-G-10% DOX-4% ZIF-8.

#### Antibacterial activities results

In terms of comparison of the antibacterial effects of nanocomposite films on *S. aureus* and *E. coli*, the most effective was CS-PEG-G-10% DOX-4% ZIF-8, followed by CS-PEG-G-10% DOX, and then CS-PEG-G-4% ZIF-8 ( $p < 0.05$ ). Both strains examined in the present study demonstrated sensitivity to DOX based on the

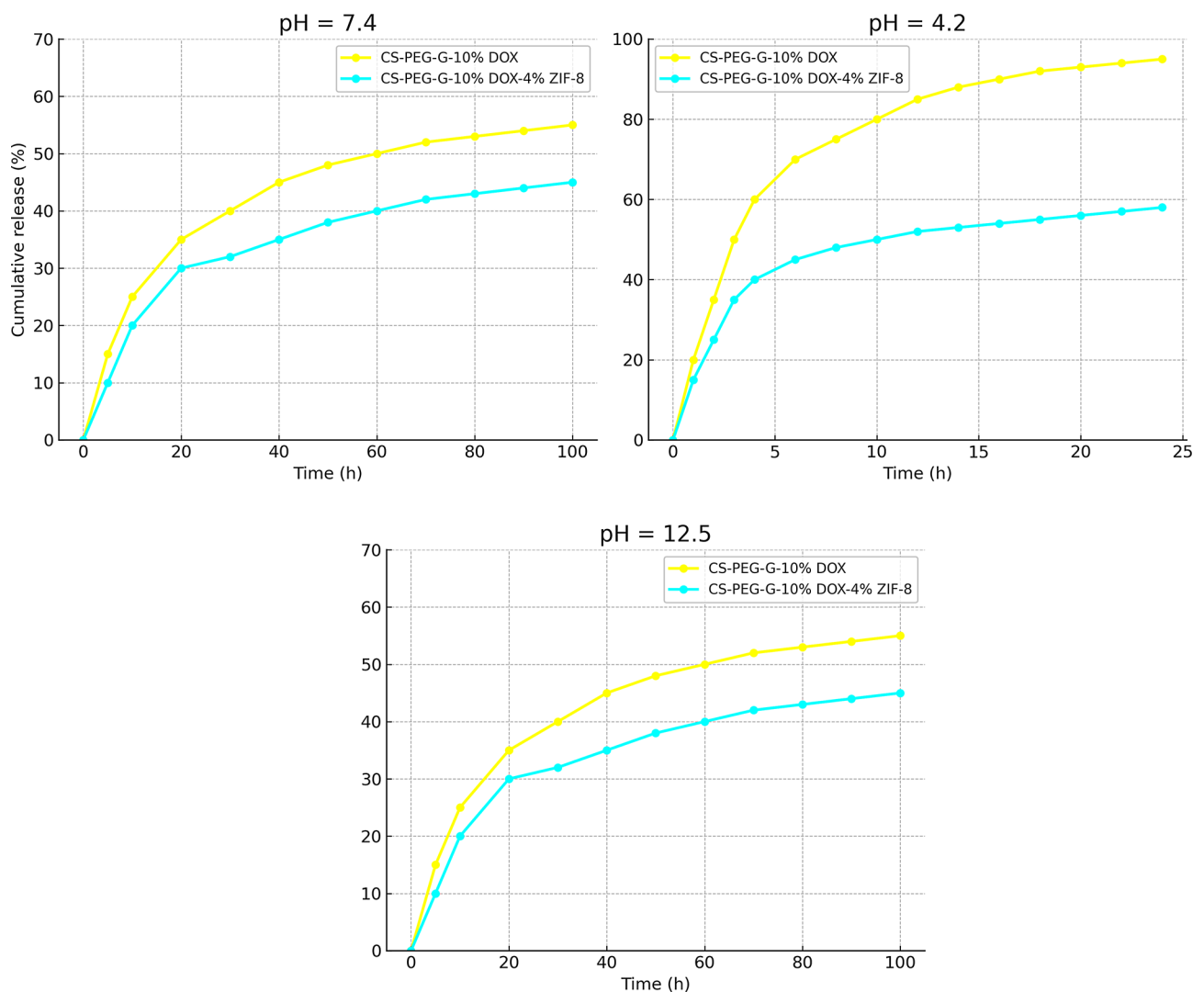


**Fig. 3** DOX Drug Release Profiles for CS-PEG-G-10% DOX and CS-PEG-G-10% DOX-4% ZIF-8 at Different pH Conditions. The cumulative release of doxycycline (DOX) from the nanocomposite films is shown over time at three different pH levels. The yellow line represents the drug release profile of CS-PEG-G-10% DOX, while the pale blue line represents CS-PEG-G-10% DOX-4% ZIF-8. The graphs illustrate the influence of pH on the release rate, with higher release percentages observed at lower pH values

antimicrobial sensitivity test conducted using the disk diffusion method.

The statistical analysis of the inhibition zones for *S. aureus* and *E. coli* across the different nanocomposite films shows a clear trend of increasing antibacterial efficacy with the addition of ZIF-8 and DOX to the CS-PEG-G matrix. The CS-PEG-G-4% ZIF-8 formulation exhibited a moderate antibacterial effect. The addition of 10% DOX further enhanced the antibacterial activity, particularly for *S. aureus*, resulting in an inhibition

zone of 22 mm. The most effective combination was CS-PEG-G-10% DOX-4% ZIF-8, which produced the most significant inhibition zones of 22.5 mm for *S. aureus* and 14 mm for *E. coli* (Fig. 4). In the disk diffusion assay, nanocomposite films exhibited a more potent antibacterial effect on *S. aureus* compared to *E. coli* ( $p < 0.05$ ).

The inhibition zone for *S. aureus* increased from 0 mm (CS-PEG-G) to 22.5 mm (CS-PEG-G-10% DOX-4% ZIF-8), representing a 2250% improvement. For *E. coli*, the inhibition zone increased from 0 mm (CS-PEG-G) to

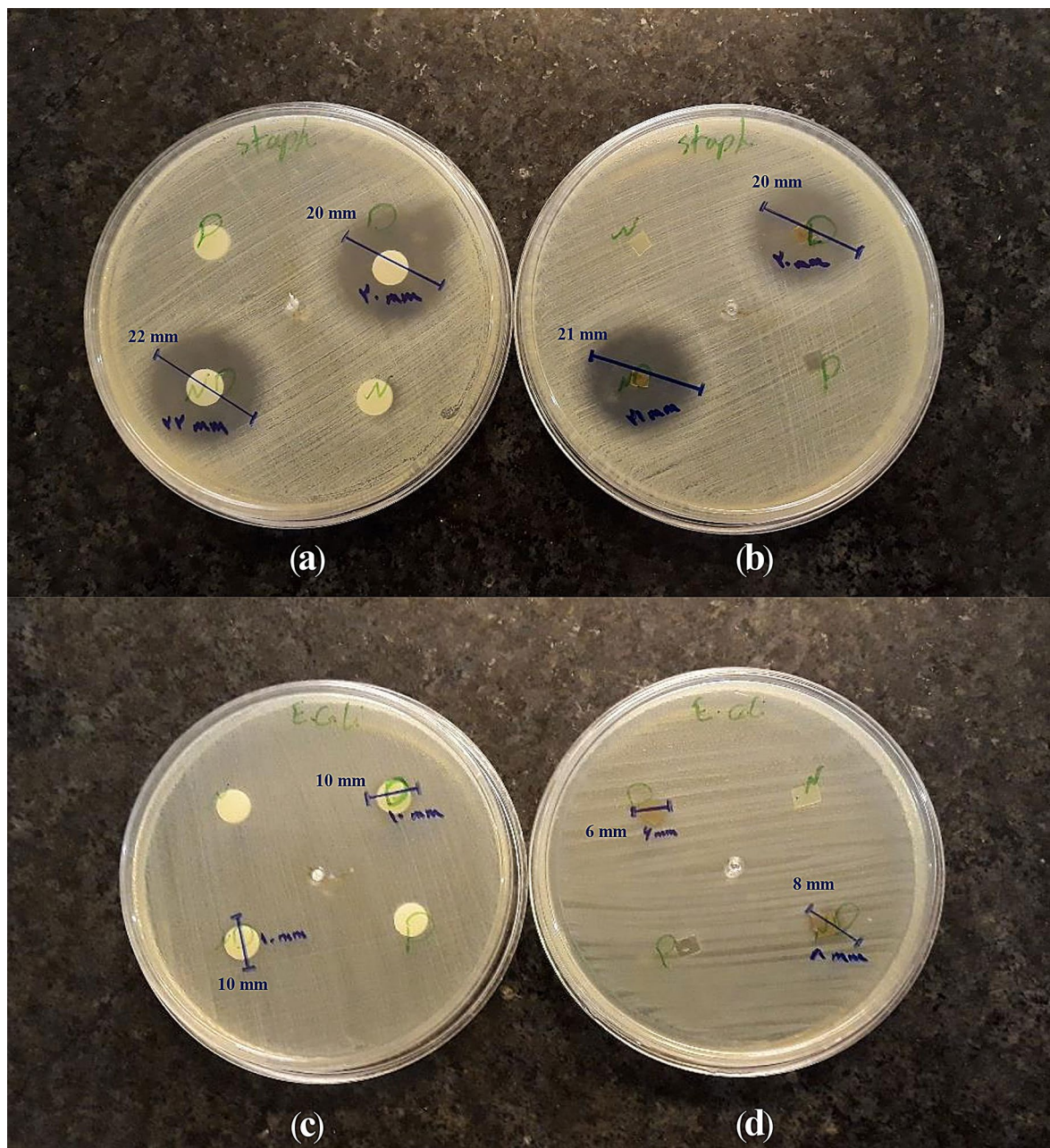


**Fig. 4** The antibacterial activity of nanocomposite films (marked by different letters) was tested against *S. aureus* (a, b) and *E. coli* (c, d) using the disc diffusion method. P: CS-PEG-G-4% ZIF-8, N: CS-PEG-G, D: CS-PEG-G-10% DOX, ND: CS-PEG-G-10% DOX-4% ZIF-8

14 mm (CS-PEG-G-10% DOX-4% ZIF-8), corresponding to a 1400% improvement. Comparing the performance of CS-PEG-G-4% ZIF-8 with CS-PEG-G-10% DOX-4% ZIF-8, the inhibition zone for *S. aureus* increased from 20 mm to 22.5 mm, indicating a 12.5% improvement. For *E. coli*, the inhibition zone increased from 10 mm to 14 mm, reflecting a 40% improvement (Fig. 5).

No inhibition of bacterial growth was observed for CS-PEG-G up to the maximum concentration evaluated (3 mg/mL). However, the incorporation of 4% ZIF-8 into the CS-PEG-G matrix significantly enhanced its antimicrobial properties, with MIC values of 0.48 mg/mL for *S. aureus* and 0.96 mg/mL for *E. coli* and MBC values of 0.96 mg/mL and 1.92 mg/mL, respectively. Further improvement was observed with the addition of 10% DOX, particularly for *S. aureus*, which showed an MIC of 0.03 mg/mL and an MBC of 0.06 mg/mL. For *E. coli*, the MIC was 0.48 mg/mL, and the MBC was 0.96 mg/mL. The combination of 10% DOX and 4% ZIF-8 exhibited the most potent antibacterial activity, with MIC values of 0.00375 mg/mL for *S. aureus* and 0.24 mg/mL for *E. coli* and MBC values of 0.0075 mg/mL and 0.48 mg/mL, respectively (Fig. 5). These results demonstrate that CS-PEG-G-10% DOX-4% ZIF-8 is the most effective formulation, showing superior bacterial inhibition at lower concentrations.

For *S. aureus*, the most synergistic interaction was observed at a concentration of 0.03 mg/mL for CS-PEG-G-10% DOX and 0.12 mg/mL for CS-PEG-G-4% ZIF-8. This combination yielded a FICI value below 0.5, suggesting a strong synergistic effect between the two nanocomposite films. Synergy was further observed over a range of concentrations, where the color gradient indicated enhanced antibacterial activity as the concentration of the two compounds increased (Fig. 6). Similarly, for *E. coli*, the green star on the heatmap marks the most

synergistic interaction, with a combination of 0.12 mg/mL CS-PEG-G-10% DOX and 0.24 mg/mL CS-PEG-G-4% ZIF-8. This combination also resulted in a FICI value below 0.5, confirming the synergistic effect against *E. coli*. Overall, the results demonstrate that the combination of CS-PEG-G-10% DOX and CS-PEG-G-4% ZIF-8 is highly synergistic against both *S. aureus* and *E. coli* ( $p < 0.05$ ), particularly at the concentrations indicated in the heatmaps (Fig. 6).

## Discussion

The findings of the current study show that incorporating DOX and ZIF-8 into the CS-PEG-G matrix significantly improves the antibacterial performance of the nano composite films against both *S. aureus* and *E. coli*. These innovative polymer nanocomposites are cost-effective and straightforward to produce [36]. The synergistic interaction between DOX and ZIF-8 observed in this study underscores their potential to combat bacterial resistance and offers a promising approach for creating more efficient antimicrobial treatments.

The nanocomposite films fabricated were uniform, flexible, and nearly transparent, with their thickness increasing as the concentration of ZIF-8 was raised. The structural, physical, and mechanical properties observed in the current investigation are consistent with findings from similar research, confirming the precise synthesis of these nanocomposite films [36, 45, 46]. The incorporation of ZIF-8 nanoparticles resulted in a reduction in the thickness of the layers containing these particles. The effect of ZIF-8 on the d-spacing (interatomic spacing) between polymer chains, and consequently on layer thickness, can be interpreted in two ways: first, interactions like intercalation between ZIF-8 nanoparticles and polymer chains may reduce the d-spacing. On the other hand, the formation of specific phases in the polymer

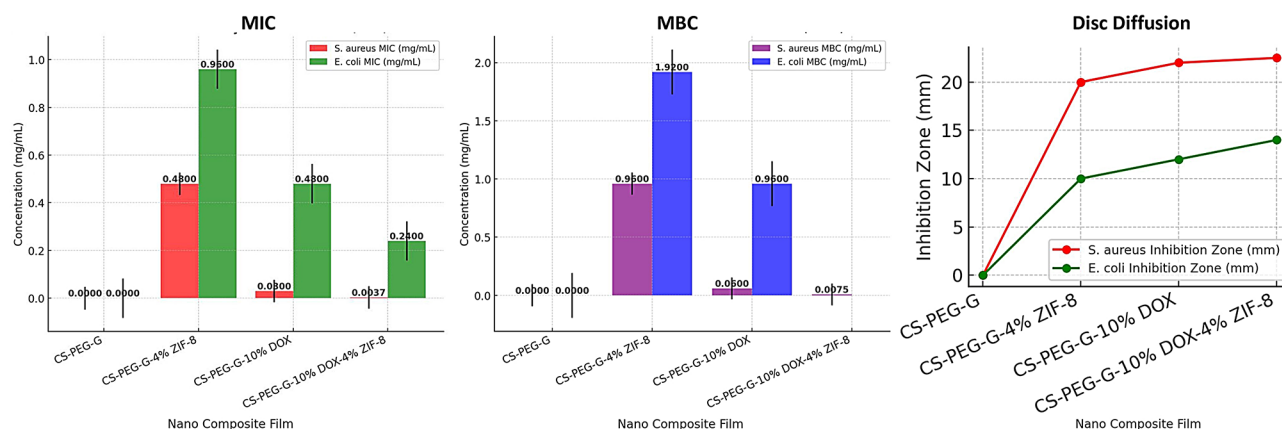


**Fig. 5** Comparative analysis of antimicrobial activity for various nanocomposite films. (Left) Minimum Inhibitory Concentration (MIC) and (Center) Minimum Bactericidal Concentration (MBC) of *S. aureus* and *E. coli* against different nano composite films. (Right) The disc diffusion method shows inhibition zones (mm) for *S. aureus* and *E. coli*. The nano composite films include CS-PEG-G, CS-PEG-G-4% ZIF-8, CS-PEG-G-10% DOX, and CS-PEG-G-10% DOX-4% ZIF-8

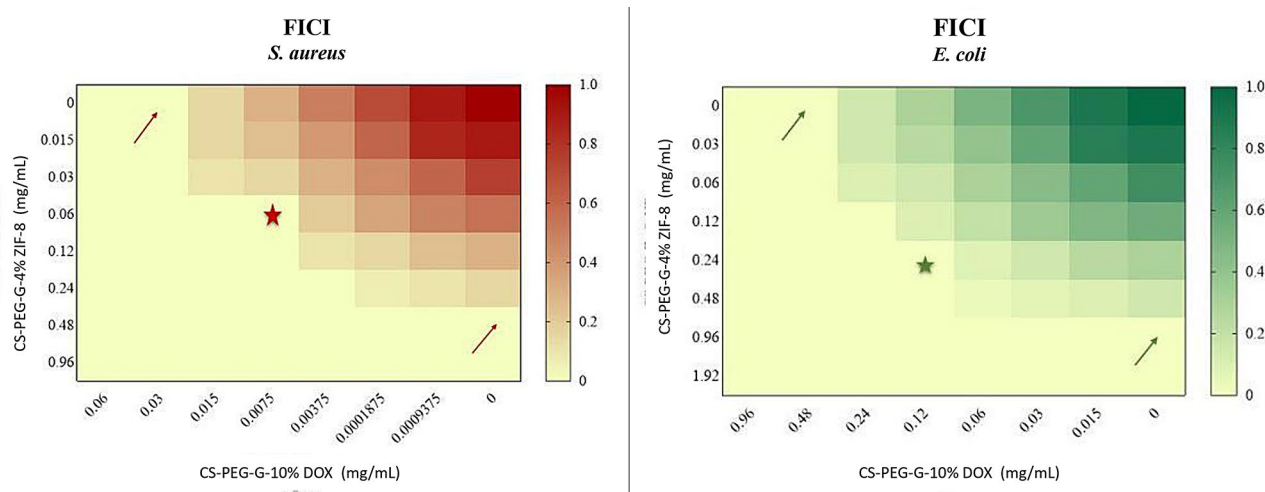


**Fig. 6** FIC heatmaps for the combination of CS-PEG-G-10% DOX and CS-PEG-G-4% ZIF-8 against *S. aureus* (left) and *E. coli* (right). The FICI values are represented by the color gradient, where darker shades indicate higher FICI values, reflecting decreased synergy between the two compounds. Red star (left) and green star (right) indicate the most synergistic concentrations for *S. aureus* and *E. coli*, respectively

matrix surrounding the ZIF-8 nanoparticles can lead to an increase in d-spacing. This is due to the filler's ability to disrupt the packing of polymer chains, a phenomenon more pronounced with higher filler concentrations [47]. In the present study, the d-spacing results indicate that the distance between polymer chains is more considerable in CS compared to PEG, likely due to increased hydration layers in CS and stronger entanglements and interactions between PEG chains. Furthermore, the addition of ZIF-8 nanoparticles and the DOX drug increased the d-spacing, suggesting decreased regularity and larger spacing between chains. These findings are consistent with the film thickness measurements observed in this study [36].

The DOX release profiles showed an initial burst release, followed by a sustained release in acidic, neutral, and alkaline conditions. This behavior likely stems from the rapid release of DOX from the polymer matrix caused by film swelling, after which the DOX trapped within the films was gradually released via diffusion. The rapid swelling of polymer matrices allows for a quick release of DOX, as observed in studies with pH-responsive microbeads [48]. After the initial burst, the remaining DOX is released gradually through diffusion, as supported by the findings on micelle-like aggregates where pH changes significantly affect release rates [49]. The release kinetics vary with pH; acidic conditions can enhance swelling and initial release, while alkaline conditions may facilitate sustained release due to polymer chain conformation changes [50]. Additionally, the steady increase in drug release observed in the ZIF-8-containing film can be attributed to the entrapment of DOX molecules within the nanoparticle pores, as well as the enhanced hydrogen bonding and electrostatic interactions between the drug

molecules and ZIF-8 nanoparticles. The dissolution of ZIF-8 and CS in acidic conditions further contributes to this release pattern [51–53].

It is noteworthy to highlight that the distinctive framework of ZIF-8 offers a large surface area and uniform porosity, along with exceptional biodegradability and high chemical and thermal stability. These characteristics, combined with the findings of this study, suggest that ZIF-8 could be an ideal candidate for developing drug delivery systems, particularly in the realm of antibiotics, aimed at combating antibiotic resistance and enhancing the efficacy of antibiotic treatments [27, 53–55]. ZIF-8 exhibits a high surface area, which allows for significant drug-loading capacity. For instance, ZIF-8-derived spherical porous carbon demonstrated a maximum drug loading of 300 mg/g for metronidazole [56]. ZIF-8 uniform porosity enables controlled drug release, which is essential for sustained therapeutic effects [57]. ZIF-8 is inherently biodegradable, which minimizes long-term toxicity in biological systems [55].

The observed result in the current study, where CS-PEG-G-10% DOX-4% ZIF-8 emerged as the most effective nanocomposite film against bacterial strains, can be attributed to the synergistic interaction between the components of the nanocomposite, particularly the ZIF-8 nanoparticles and DOX. ZIF-8, a type of MOF, exhibits high surface area and porosity, facilitating the sustained release of antimicrobial agents like DOX, thus enhancing the antibacterial effects. Several recent studies have highlighted the efficacy of ZIF-8 in enhancing antibacterial properties due to its ability to disrupt bacterial cell walls and its potential for encapsulating antibacterial agents for a controlled release [58]. For instance, In the study by Saif et al., zeolitic imidazole framework-8

(ZIF-8) was combined with a novel *Cordia myxa* extract to create a CME@ZIF-8 nanocomposite, which demonstrated superior antibacterial activity against *S. aureus* and *E. coli*. Their results indicated that CME@ZIF-8 was significantly more effective than ZIF-8 alone and the commercially available antibiotic Ciprofloxacin. This improvement was attributed to the generation of reactive oxygen species (ROS) by CME@ZIF-8, which destroyed bacterial cells [59]. In the referenced study, similar to the current research, the nanocomposite was analyzed using techniques such as UV-vis, XRD, and SEM. However, a key distinction in the present study is the deliberate effort to examine each component of the nanocomposite separately, as thoroughly as possible. The 2024 study by Sevimli-Yurttas et al. employed similar methodologies to those used in the present research to examine ZIF-8 nanocomposites. It also emphasized the potential applications of these nanocomposites as effective antimicrobial delivery agents [60].

In the study by Raju et al., zeolitic imidazole framework-8 (ZIF-L) was combined with *Leucas aspera* extract to create an LA@ZIF-L nano framework. This composite was then evaluated for its antimicrobial and anticancer properties. The results indicated that the LA@ZIF-L nano framework showed significant antibacterial potential against a variety of bacterial strains (*Bacillus subtilis*, *S. aureus*, *Klebsiella pneumoniae*, and *Pseudomonas aeruginosa*), with inhibition zones ranging from 17 mm to 21 mm. Additionally, it demonstrated potent anticancer activity against A549 cells, with an IC<sub>50</sub> value of  $42.61 \pm 0.05$  µg/mL. Furthermore, its biocompatibility was confirmed through a toxicity assay on *Artemia salina*, with an LC<sub>50</sub> value of  $135.33 \pm 2.00$  µg/ml, highlighting the potential of ZIF-L as an effective drug delivery system for both bacterial infection and cancer treatment. Similarly, the present study showed that ZIF-8, when combined with DOX, enhanced the antimicrobial potential, particularly against *S. aureus* and *E. coli*. The use of ZIF-8 as a carrier for drug delivery in both studies reinforces its effectiveness in enhancing antimicrobial activity, aligning with the findings of Raju et al. [61].

In Wang et al.'s study, the ZIF-8 was combined with polydopamine (PDA) to create a ZIF-8@PDA composite. This combination enhanced the water stability, photocatalytic, and photothermal capabilities of ZIF-8. The composite was further incorporated into carboxylated SC (CCS) films, demonstrating excellent antibacterial performance with a 99% bacterial inhibition rate in vitro. Additionally, these ZIF-8@PDA-CCS films were influential in completely suppressing bacteria in infected wounds, suggesting their potential use as antibacterial dressings. In the present study, a similar approach was taken by incorporating ZIF-8 into CS-PEG-G films, which demonstrated a significant antibacterial effect. Such findings

highlight ZIF-8's versatile role as an effective drug delivery system for treating infections, aligning with Wang et al.'s findings on its antimicrobial potential [62].

In the study by Sun et al., a Ciprofloxacin-loaded ZIF (CI@ZIF-90) was created for pH-responsive drug delivery, with an emphasis on sepsis treatment. Drug release was examined at various pH levels, revealing that 98% of the drug was released within 72 h at pH 5.0. The study included a variety of in vitro and in vivo tests such as well-diffusion, MIC, and biofilm assays to verify CI@ZIF-90's antimicrobial efficacy against pathogens, as well as biocompatibility evaluations. Compared to the present study, both investigations leverage ZIF-based nanocomposites for antimicrobial purposes. In a manner similar to the present study, Sun et al. observed the highest drug release at a neutral pH level. This comparison indicates that in both studies, the nanocomposites demonstrated their most effective release of active agents under neutral conditions, which is critical for optimizing drug delivery in specific biological environments [63].

At the nanoscale, materials often exhibit increased surface area, altered electronic properties, and enhanced interactions with biological systems. In the case of CS-PEG-G-10% DOX-4% ZIF-8, the nanoscale formulation likely enhances the contact between the antibacterial agents and the bacterial cells, allowing for more efficient penetration and interaction with bacterial membranes. This increased surface area and the ability to deliver the active components directly to the target site amplify the synergistic effects of ZIF-8 and Dox. Moreover, the nanoparticle formulation can improve the stability and bioavailability of the active agents, ensuring that they remain effective over a more extended period and at lower concentrations [64–66]. The significant enhancement of antibacterial activity in the nanoparticle state highlights the importance of nanoscale formulation in maximizing the therapeutic potential of combined agents [67]. This finding is particularly relevant in the context of developing new strategies to combat bacterial infections, especially with the growing concern about antibiotic resistance [68, 69].

In the current research, nanocomposite films demonstrated a more substantial antibacterial impact on gram-positive bacteria than gram-negative ones. This variation in antibacterial effectiveness can be linked to the structural and chemical characteristics of both the bacteria and the ZIFs. Gram-positive bacteria tend to exhibit a greater affinity for metals compared to Gram-negative bacteria due to differences in the molecular composition of their cell walls. Gram-positive bacteria have a robust and thick peptidoglycan layer, whereas Gram-negative bacteria lack this structure. Instead, Gram-negative bacteria possess a 10 nm thick lipopolysaccharide (LPS) layer covering the outer peptidoglycan layer. This LPS layer

acts as a barrier, hindering the penetration of nanoparticles into the cell wall [2, 55]. The findings of the present study closely mirrored another study, where ZIF-8 demonstrated a remarkable antibacterial effect, achieving a 99% inhibition rate against gram-positive bacteria while showing comparatively lower efficacy against gram-negative bacteria [62]. Such findings suggest that Gram-negative bacteria exhibit more excellent nanoparticle resistance than Gram-positive bacteria. According to Ibraheem et al., nanomaterials incorporating Zinc Oxide (ZnO) nanoparticles demonstrated more potent antibacterial effects against gram-positive bacteria than gram-negative ones [2]. It is further noted that incorporating ZIFs into polymeric matrices like CS enhances their stability and boosts their antibacterial effectiveness, particularly against Gram-positive bacteria. While ZIFs show significant potential as antibacterial agents, the inherent resistance mechanisms of gram-negative bacteria, such as their outer membrane barrier, may limit the effectiveness of ZIFs against them. Further research is needed to optimize formulations for broader antibacterial applications [55, 70].

The antibacterial mechanism is attributed to the release of zinc ions, which compromise bacterial cell membranes. Kermanshahi et al. revealed that ZIF-8 exhibited superior antibacterial effectiveness compared to ZIF-4, ZIF-7, and ZnO nanoparticles, primarily due to its zinc ion release. In this study, ZIF-8 showed the most potent antibacterial activity among the ZIFs tested, surpassing both ZIF-7 and ZnO nanoparticles derived from the framework [71]. These observations are consistent with the present study's findings, which also demonstrate that ZIF-8-based nanocomposites are highly effective against *S. aureus* and *E. coli*.

Nano-antibiotics are promising platforms for mitigating antibiotic resistance and their adverse side effects [2]. Infectious diseases are the primary cause of death globally. Nanotechnology offers a promising avenue for combating drug-resistant microbial infections. While traditional antibiotics have been effective in controlling microbial growth and eliminating pathogens, their effectiveness is increasingly hampered by the development of resistance and associated side effects. The advent of nanotechnology has revolutionized antimicrobial therapy through the use of nanoparticles. These nanoparticles play a crucial role in diagnosing and treating infectious diseases by minimizing side effects and enhancing targeted drug delivery to affected tissues [72].

The current study highlights the efficacy of CS-PEG-G in generating DOX and ZIF-8 nanoparticle coatings, with ZIF-8 showing significant promise as a drug delivery system. However, for its practical application, further modifications are required to optimize stability, mitigate toxicity, and ensure the protection of drugs

during delivery. These modifications are also essential for enabling controlled and sustained drug release at targeted sites or under specific conditions. The incorporation of such strategies significantly enhances the potential of ZIF-8 as an effective drug delivery carrier. Commonly, surface modification of ZIF-8 nanoparticles includes the addition of PEG or carboxylated PEG (PEG2000-COOH), which helps to minimize non-specific interactions with plasma proteins, thereby prolonging circulation time [73]. PEG, a polymer of natural or synthetic origin, proved effective in this role, rendering ZIF-8 biologically friendly and reducing their cytotoxicity. PEG serves as an intermediary agent, acting as a molecular spacer and linker to attach DOX molecules to the surfaces of ZIF-8 nanoparticles. Other biopolymers, such as hyaluronic acid (HA), CS, and polyvinylpyrrolidone (PVP), are also used for surface functionalization. Moreover, combining ZIF-8 nanoparticles with PEG broadens their utility across various fields, including medicine, therapy, agriculture, and industry [2, 73, 74].

In the study by Mazloom-Jalali, the fabricated CS-PEG containing ZIF-8 nanoparticles exhibited significant mechanical strength, swelling behavior, and controlled drug release, making them promising for wound dressing applications. The sustained drug release of Cephalexin in different pH environments (acidic, neutral, alkaline) aligns with the present study's findings, which also observed the advantages of incorporating ZIF-8 nanoparticles into nanocomposite films for antibacterial effectiveness and controlled drug delivery. Additionally, the enhanced mechanical properties and cell viability demonstrated in Mazloom-Jalali et al.'s study further support the selection of films containing 4% ZIF-8 in current research. This percentage of ZIF-8 was chosen for its optimal performance, as it presented balanced mechanical strength, swelling capacity, and drug release, making it the best candidate for further applications. The ability of ZIF-8 to improve these parameters reinforces the decision to include 4% ZIF-8 in present nanocomposite films, especially for biomedical uses. The film's superior characteristics in drug release, swelling, and cell compatibility underscore the broader potential of ZIF-8 as a key component in medical applications [36].

The superior antibacterial performance of CS-PEG-G-10% DOX-4% ZIF-8, as indicated by their MIC and MBC values, aligns with findings from recent studies. For instance, research by Ray Chowdhuri et al. demonstrated that a ZnO-decorated chitosan-graphene oxide nanocomposite exhibited enhanced antimicrobial activity, achieving low MIC values for both *E. coli* and *S. aureus*, attributed to reactive ROS generation and oxidative damage. This highlights the importance of combining ZnO with other antimicrobial agents to boost efficacy [75]. Furthermore, a review by Sirelkhatim et al. emphasized

the role of ZnO nanoparticles size, shape, and synthesis methods in determining their antibacterial properties, suggesting that incorporating ZnO with other active agents, such as Dox, can enhance their antibacterial effects against resistant pathogens [76].

The FICI values obtained in the current study reveal the synergistic effects of the CS-PEG-G-10% DOX-4% ZIF-8 nanocomposite films. These results suggest a more potent antibacterial effect against *S. aureus* than *E. coli*, as evidenced by the lower FICI and MIC values for *S. aureus*. This observation aligns with the findings of other studies indicating that the combination of antimicrobial agents can significantly enhance antibacterial efficacy. For example, a recent study on the synergistic action between copper oxide nanoparticles and anthraquinone-2-carboxylic acid against *S. aureus* demonstrated that the combined use of nanoparticles and other antimicrobial agents can reduce resistance and improve antibacterial outcomes [77]. Additionally, research on the green synthesis of ZIF-8 nanoparticles showed that incorporating ZIF-8 with other antimicrobial agents improves effectiveness against a broad spectrum of pathogens, including MDR bacteria [78].

Furthermore, the investigations carried out on ZIF-8 nanoparticles highlighted the importance of nanoparticles morphology, size, and combination with other agents in enhancing antibacterial properties. The morphology and size of nanoparticles significantly influence their antibacterial efficacy. Smaller, well-distributed nanoparticles exhibit enhanced interaction with bacterial membranes, leading to improved antibacterial activity [79]. ZIF-8's unique structure allows for the effective loading of therapeutic agents, enhancing their release and activity against resistant strains [80]. Multi-agent approaches, including the use of bio-nanomaterials, are crucial in addressing the global challenge of antimicrobial resistance. The integration of various agents can mitigate resistance mechanisms, prolonging the effectiveness of existing antibiotics and reducing side effects [81]. While the focus on ZIF-8 and DOX is promising, it is essential to consider the potential cytotoxicity and environmental impact of these nanocomposites, necessitating further research into their safety profiles and regulatory considerations.

The emergence of bacterial resistance to antibiotics is poised to become one of the most significant global health challenges [1]. The efficacy of many antimicrobial drugs is limited due to low solubility, toxicity to healthy tissues, and rapid degradation and clearance from the bloodstream. However, nanoantibiotics offer a promising solution to these problems due to their higher surface-to-volume ratio and unique physicochemical properties. Specific nanoparticles possess inherent antimicrobial properties, enabling them to address these limitations effectively. Consequently, the scope of pharmaceutical

nanotechnology is expanding rapidly, and it is anticipated that more “nano drugs” will be developed and utilized in the future [28, 72, 82, 83]. Incorporating DOX and ZIF-8 in CS-PEG-G nanocomposites significantly enhances their antibacterial effects.

## Conclusions

The present study highlights the remarkable antibacterial potential of CS-PEG-G-ZIF-8-Dox nanocomposites, with a particular effectiveness against Gram-positive bacteria such as *S. aureus*. The synergistic integration of ZIF-8 and Dox within the CS-PEG-G matrix significantly enhances antibacterial activity, resulting in reduced MIC and MBC values, thus improving overall efficacy. Based on the comprehensive evaluation of morphological, mechanical, antibacterial, and drug release properties, the CS-PEG-G-10% DOX-4% ZIF-8 nanocomposite stands out as a promising candidate for antibacterial applications. These findings underscore the potential of this nanocomposite for developing more potent antibacterial therapies, mainly targeting multidrug-resistant pathogens.

## Abbreviations

MDR	Multidrug-resistant
MRSA	Methicillin-resistant <i>Staphylococcus aureus</i>
MOF	Metal-organic framework
NDDS	Nanostructured Drug Delivery Systems
LPS	Lipopolysaccharide
ZIF-8	Zeolitic imidazolate framework-8
DOX	Doxycycline (a broad-spectrum antibiotic)
PEG	Polyethylene glycol
ZnO	Zinc oxide
CS	Chitosan
XRD	X-ray diffraction
ATCC	American Type Culture Collection
MHB	Mueller Hinton Broth
MHA	Mueller Hinton Agar
CFU	Colony Forming Unit
CLSI	Clinical and Laboratory Standards Institute
MIC	Minimum Inhibitory Concentration
MBC	Minimum Bactericidal Concentration
ANOVA	Analysis of variance
FICI	Fractional inhibitory concentration index
UTM	Universal Testing Machine
ROS	Reactive Oxygen Species

## Acknowledgements

The authors are sincerely grateful to the Laboratory of Microbiology and Immunology, Faculty of Veterinary Medicine, University of Tehran, Iran.

## Author contributions

B.N.F. and R.Y. devised the project, developed the main conceptual ideas, and outlined the proof. B.N.F., A.M.J., F.J., and R.Y. handled most of the technical details and performed the numerical calculations for the proposed experiment. All authors conducted the experiments and analyzed the data. B.N.F. and S.M.J. critically revised the manuscript for important intellectual content. S.M.J. wrote the manuscript, drafting the initial text, and integrating feedback from all co-authors to produce the final version. All authors provided critical feedback and contributed to shaping the research, analysis, and manuscript.

## Funding

This research received NO specific grant from any funding agency in the public, commercial, or not-for-profit sectors.

### Data availability

The datasets used and/or analyzed during the current study are available from the corresponding author upon reasonable request.

### Declarations

#### Ethics approval and consent to participate

Not applicable. This article does not include any studies conducted by the authors involving human participants or animals. All research and analyses presented are based on experimental methods and data that do not include human or animal subjects. This disclaimer ensures compliance with ethical standards and regulations regarding research involving human and animal participants.

#### Consent for publication

Not applicable.

#### Competing interests

The authors declare no competing interests.

Received: 10 October 2024 / Accepted: 17 February 2025

Published online: 20 February 2025

### References

1. Tang KWK, Millar BC, Moore JE. Antimicrobial Resistance (AMR). *Br J Biomed Sci* 2023;80.
2. Ibraheem DR, Alwas NGA, Abbood SH, Nasser SM, Sulaiman GM, Jabir MS, Mohammed HA, Fawzi HA. Nystatin-Based Zinc Oxide Nanoparticles Coated with Polyethylene Glycol for Enhancing the Antibacterial Activity Against Some Resistance Pathogenic Bacteria. *BioNanoScience* 2024.
3. Aldarhami A, Bazaid AS, Alhamed AS, Alghaith AF, Ahamad SR, Alasmrri YA, Alharazi T, Snoussi M, Qanash H, Alamri A, et al. Antimicrobial potential of *Pithecellobium dulce* seed extract against pathogenic Bacteria: in Silico and in Vitro evaluation. *Biomed Res Int*. 2023;2023(1):2848198.
4. Lade H, Kim J-S. Bacterial targets of antibiotics in Methicillin-Resistant *Staphylococcus aureus*. *Antibiotics*. 2021;10(4):398.
5. Mohammed HA, Amin MA, Zayed G, Hassan Y, El-Mokhtar M, Saddik MS. In vitro and in vivo synergistic wound healing and anti-methicillin-resistant *Staphylococcus aureus* (MRSA) evaluation of liquorice-decorated silver nanoparticles. *J Antibiot*. 2023;76(5):291–300.
6. Ren G, Clancy C, Tamer TM, Schaller B, Walker GM, Collins MN. Cinnamyl O-amine functionalized Chitosan as a new excipient in direct compressed tablets with improved drug delivery. *Int J Biol Macromol*. 2019;141:936–46.
7. Borbolla-Jiménez FV, Peña-Corona SI, Farah SJ, Jiménez-Valdés MT, Pineda-Pérez E, Romero-Montero A, Del Prado-Audelo ML, Bernal-Chávez SA, Magaña JJ, Leyva-Gómez G: films for Wound Healing fabricated using a solvent casting technique. In: *Pharmaceutics* 15;2023.
8. Alemu Reta B, K MB, Tesfaye T. Smart and intelligent biomaterials for novel applications – a review. *Int J Polym Mater Polym Biomaterials* 2024:1–19.
9. Niaraki NJ, Jamshidi S, Fasaei BN, Joghataei SM. Antibacterial effects of chitosan-based hydrogels containing *Trachyspermum ammi* essential oil on pathogens isolated from dogs with otitis externa. *BMC Vet Res*. 2024;20(1):130.
10. Park H, Otte A, Park K. Evolution of drug delivery systems: from 1950 to 2020 and beyond. *J Controlled Release*. 2022;342:53–65.
11. Shanmuganathan R, Edison TNJ, LewisOscar F, Kumar P, Shanmugam S, Pugazhendhi A. Chitosan nanopolymers: an overview of drug delivery against cancer. *Int J Biol Macromol*. 2019;130:727–36.
12. Gheorghita D, Moldovan H, Robu A, Bița A-I, Grosu E, Antoniac A, Corneschi I, Antoniac I, Bodog AD, Băcilă CI. Chitosan-based biomaterials for hemostatic applications: a review of recent advances. In: *Int J Mol Sci* 24;2023.
13. Kolawole OM, Lau WM, Khutoryanskiy VV. Synthesis and Evaluation of Boronated Chitosan as a Mucoadhesive Polymer for Intravesical Drug Delivery. *J Pharm Sci*. 2019;108(9):3046–53.
14. Chen H, Cheng J, Ran L, Yu K, Lu B, Lan G, Dai F, Lu F. An injectable self-healing hydrogel with adhesive and antibacterial properties effectively promotes wound healing. *Carbohydr Polym*. 2018;201:522–31.
15. Perera AAPR, Madhushani KAU, Kumar A, Gupta RK. Metal-organic frameworks for wastewater treatment: recent developments, challenges, and future prospects. *Chemosphere*. 2023;339:139713.
16. Li D, Yadav A, Zhou H, Roy K, Thanasekaran P, Lee C. Advances and applications of Metal-Organic frameworks (MOFs) in Emerging technologies: a Comprehensive Review. *Global Challenges*. 2024;8(2):2300244.
17. Adhikari C, Mishra A, Nayak D, Chakraborty A. Metal organic frameworks modified mesoporous silica nanoparticles (MSN): a nano-composite system to inhibit uncontrolled chemotherapeutic drug delivery from Bare-MSN. *J Drug Deliv Sci Technol*. 2018;47:1–11.
18. Xing F, Xu J, Zhou Y, Yu P, Zhe M, Xiang Z, Duan X, Ritz U. Recent advances in metal-organic frameworks for stimuli-responsive drug delivery. *Nanoscale*. 2024;16(9):4434–83.
19. Ezike TC, Okpala US, Onoja UL, Nwike CP, Ezeako EC, Okpara OJ, Okoroafor CC, Eze SC, Kalu OL, Odoh EC, et al. Advances in drug delivery systems, challenges and future directions. *Heliyon*. 2023;9(6):e17488.
20. Li C, Wang J, Wang Y, Gao H, Wei G, Huang Y, Yu H, Gan Y, Wang Y, Mei L, et al. Recent progress in drug delivery. *Acta Pharm Sinica B*. 2019;9(6):1145–62.
21. Vatanparast M, Shariatinia Z. Revealing the role of different nitrogen functionalities in the drug delivery performance of graphene quantum dots: a combined density functional theory and molecular dynamics approach. *J Mater Chem B*. 2019;7(40):6156–71.
22. Jin C-X, Shang H-B. Synthetic methods, properties and controlling roles of synthetic parameters of zeolite imidazole framework-8: a review. *J Solid State Chem*. 2021;297:122040.
23. Kaur H, Mohanta GC, Gupta V, Kukkar D, Tyagi S. Synthesis and characterization of ZIF-8 nanoparticles for controlled release of 6-mercaptopurine drug. *J Drug Deliv Sci Technol*. 2017;41:106–12.
24. Hao C, Zhou D, Xu J, Hong S, Wei W, Zhao T, Huang H, Fang W. One-pot synthesis of Vancomycin-encapsulated ZIF-8 nanoparticles as multivalent and photocatalytic antibacterial agents for selective-killing of pathogenic gram-positive bacteria. *J Mater Sci*. 2021;56(15):9434–44.
25. Costa BA, Abuçafy MP, Barbosa TW, da Silva BL, Fulindi RB, Isquibola G, da Costa PI, Chiavacci LA. ZnO@ZIF-8 nanoparticles as Nanocarrier of Ciprofloxacin for Antimicrobial Activity. In: *Pharmaceutics* 2023;15.
26. Azizi Vahed T, Naimi-Jamal MR, Panahi L. Alginate-coated ZIF-8 metal-organic framework as a green and bioactive platform for controlled drug release. *J Drug Deliv Sci Technol*. 2019;49:570–6.
27. Soomro NA, Wu Q, Amur SA, Liang H, Ur Rahman A, Yuan Q, Wei Y. Natural drug physcion encapsulated zeolitic imidazolate framework, and their application as antimicrobial agent. *Colloids Surf B*. 2019;182:110364.
28. Saliy O, Popova M, Tarasenko H, Getalo O. Development strategy of novel drug formulations for the delivery of doxycycline in the treatment of wounds of various etiologies. *Eur J Pharm Sci*. 2024;195:106636.
29. Malek AE, Granwehr BP, Kontoyiannis DP. Doxycycline as a potential partner of COVID-19 therapies. *IDCases*. 2020;21:e00864.
30. Feitosa RC, Ishikawa ESA, Silva MFAd S-J, AAd, Oliveira-Nascimento L. Five decades of doxycycline: does nanotechnology improve its properties? *Int J Pharm*. 2022;618:121655.
31. Carvalho Feitosa R, Souza Ribeiro Costa J, van Vliet Lima M, Sawa Akioka Ishikawa E, Cogo Müller K, Bonin Okasaki F, Sabadini E, Garnerio C, Longhi MR, Lavayen V, et al. Supramolecular arrangement of doxycycline with Sulfobutylether- $\beta$ -Cyclodextrin: impact on Nanostructuration with Chitosan, Drug Degradation and Antimicrobial Potency. *Pharmaceutics*. 2023;15(4):1285.
32. Castro-Pastrana LI, Angulo Molina A, Flood-Garibay JA, Quintana-Romero DA, Crespo-Morán P, Méndez-Rojas MA. Recent Advances on Nanostructured Materials for Drug Delivery and Release. In: *Nanopharmaceuticals: Principles and Applications Vol 2*. Edited by Yata VK, Ranjan S, Dasgupta N, Lichtfouse E. Cham: Springer International Publishing; 2021:319–360.
33. Kadhum WN, Zaidan IA. The synergistic effects of chitosan-alginate nanoparticles loaded with doxycycline antibiotic against multidrug resistant *proteus mirabilis*, *Escherichia coli* and *enterococcus faecalis*. *Iraqi J Sci*. 2020;61(12):3187–99.
34. Kohsari I, Shariatinia Z, Pourmortazavi SM. Antibacterial electrospun chitosan-polyethylene oxide nanocomposite mats containing ZIF-8 nanoparticles. *Int J Biol Macromol*. 2016;91:778–88.
35. Cravillon J, Münzer S, Lohmeier S-J, Feldhoff A, Huber K, Wiebcke M. Rapid Room-Temperature synthesis and characterization of nanocrystals of a prototypical Zeolitic Imidazolate Framework. *Chem Mater*. 2009;21(8):1410–2.
36. Mazloom-Jalali A, Shariatinia Z, Tamai IA, Pakzad S-R, Malakootikhah J. Fabrication of chitosan-polyethylene glycol nanocomposite films containing

- ZIF-8 nanoparticles for application as wound dressing materials. *Int J Biol Macromol.* 2020;153:421–32.
37. CLSI. *Performance Standards for Antimicrobial Disk Susceptibility Tests*. 14th ed. CLSI standard M02. In: Clinical and Laboratory Standards Institute; 2024.
  38. CLSI. *Performance Standards for Antimicrobial Disk Susceptibility Tests*. 34th ed. CLSI standard M100. In: Clinical and Laboratory Standards Institute; 2024.
  39. Azizi-Lalabadi M, Ehsani A, Divband B, Alizadeh-Sani M. Antimicrobial activity of Titanium dioxide and zinc oxide nanoparticles supported in 4A zeolite and evaluation the morphological characteristic. *Sci Rep.* 2019;9(1):17439.
  40. Arul Selvaraj RC, Rajendran M, Nagaiah HP. Re-potentialization of  $\beta$ -Lactam Antibiotic by Synergistic Combination with Biogenic Copper Oxide Nanocubes against Biofilm forming Multidrug-resistant Bacteria. *Molecules.* 2019;24(17):3055.
  41. Hussain MA, Ahmed D, Anwar A, Perveen S, Ahmed S, Anis I, Shah MR, Khan NA. Combination therapy of clinically approved antifungal drugs is enhanced by conjugation with Silver Nanoparticles. *Int Microbiol.* 2019;22(2):239–46.
  42. Masoudi M, Mashreghi M, Zenhari A, Mashreghi A. Combinational antimicrobial activity of biogenic TiO<sub>2</sub> NP/ZnO NPs nanoantibiotics and Amoxicillin-clavulanic acid against MDR-pathogens. *Int J Pharm.* 2024;652:123821.
  43. Ray M, Pal K, Anis A, Banthia AK. Development and characterization of Chitosan-based polymeric hydrogel membranes. *Des Monomers Polym.* 2010;13(3):193–206.
  44. Liu H, Xie W-Y, Song F, Wang X-L, Wang Y-Z. Constructing hierarchically hydrophilic/superhydrophobic ZIF-8 pattern on soy protein towards a biomimetic efficient water harvesting material. *Chem Eng J.* 2019;369:1040–8.
  45. Sadiq S, Khan I, Humayun M, Wu P, Khan A, Khan S, Khan A, Khan S, Alanazi AF, Bououdina M. Synthesis of metal–Organic Framework-based ZIF-8@ZIF-67 nanocomposites for antibiotic decomposition and antibacterial activities. *ACS Omega.* 2023;8(51):49244–58.
  46. Yurtsever HA, İloğlu O. Preparation of transparent ZIF-8/TiO<sub>2</sub> Nanocomposite Thin films for Photocatalytic Applications. *Bitlis Eren Üniversitesi Fen Bilimleri Dergisi.* 2023;12(3):764–72.
  47. Ding X, Li X, Zhao H, Wang R, Zhao R, Li H, Zhang Y. Partial pore blockage and polymer chain rigidification phenomena in PEO/ZIF-8 mixed matrix membranes synthesized by in situ polymerization. *Chin J Chem Eng.* 2018;26(3):501–8.
  48. Rathnam SR, Reddy OS, Patwari SB. Development and characterization of pH-responsive polymeric microbeads intercalated with montmorillonite for controlled release of doxorubicin. *Int J Appl Pharm.* 2023;15(3):247–53.
  49. Espinola-Portilla F, d'Orlyé F, Triapiella-Alfonso L, Gutiérrez-Granados S, Ramírez-García G, Varenne A. Rational understanding of Loading and Release of Doxorubicin by UV-Light- and pH-Responsive poly(NIPAM-co-SPMA) micelle-like aggregates. *Mol Pharm.* 2023;20(3):1490–9.
  50. Li X, Auepattana-Aumrung K, Butt H-J, Crespy D, Berger R. Fast-release kinetics of a pH-responsive polymer detected by dynamic contact angles. *J Chem Phys.* 2023;158(14):144901.
  51. Shariatnia Z, Zahraee Z. Controlled release of metformin from chitosan-based nanocomposite films containing mesoporous MCM-41 nanoparticles as novel drug delivery systems. *J Colloid Interface Sci.* 2017;501:60–76.
  52. Shitole AA, Raut PW, Sharma N, Giram P, Khandwekar AP, Garnaik B. Electrospun polycaprolactone/hydroxyapatite/ZnO nanofibers as potential biomaterials for bone tissue regeneration. *J Mater Science: Mater Med.* 2019;30(5):51.
  53. Shitole AA, Giram PS, Raut PW, Rade PP, Khandwekar AP, Sharma N, Garnaik B. Clopidogrel eluting electrospun polyurethane/polyethylene glycol thromboresistant, hemocompatible nanofibrous scaffolds. *J Biomater Appl.* 2019;33(10):1327–47.
  54. Du X, Liu Y, Wang X, Yan H, Wang L, Qu L, Kong D, Qiao M, Wang L. Injectable hydrogel composed of hydrophobically modified chitosan/oxidized-dextran for wound healing. *Mater Sci Engineering: C.* 2019;104:109930.
  55. Wang Y, Zeng M, Fan T, Jia M, Yin R, Xue J, Xian L, Fan P, Zhan M. Biomimetic ZIF-8 nanoparticles: a Novel Approach for Biomimetic Drug Delivery systems. *Int J Nanomed.* 2024;19(null):5523–44.
  56. Wu D, Lin H, Ren X, Qian J, Ma N, Dai W. ZIF-8 derived spherical porous carbon as an efficient sustained-release carrier for nitroimidazole drugs. *Mater Today Chem.* 2024;38:102057.
  57. Li Z, Shao Y, Yang Y, Zan J. Zeolitic imidazolate framework-8: a versatile nano-platform for tissue regeneration. *Front Bioeng Biotechnol* 2024;12.
  58. Li Z, Zhao T, Li J, Yu Q, Feng Y, Xie Y, Sun P. Nanomedicine based on Natural products: improving clinical application potential. *J Nanomaterials.* 2022;2022(1):3066613.
  59. Saif MS, Hasan M, Zafar A, Ahmed MM, Tariq T, Waqas M, Hussain R, Zafar A, Xue H, Shu X. Advancing Nanoscale Science: synthesis and bioprinting of Zeolitic Imidazole Framework-8 for enhanced anti-infectious therapeutic efficacies. In: *Biomedicines* 2023;11.
  60. Sevimli-Yurttas Z, Moreira RG, Castell-Perez E. Aggregation and Sedimentation Stability of Nanoscale Zeolitic Imidazolate Framework (ZIF-8) Nanocomposites for Antimicrobial Agent Delivery Applications. *Nano Select* 2024;n/a(n/a):e202400029.
  61. Raju P, Muthushanmugam M, Rengasamy Lakshminarayanan R, Natarajan S. One-pot synthesis of Zeolitic Imidazole Nanoframeworks with Encapsulated Leucas Aspera Leaf Extract: Assessment of Anticancer and Antimicrobial activities. *J Cluster Sci.* 2023;34(6):2977–89.
  62. Wang X, Ren M, Wang N, Ling J, He Y, Huang S. Ouyang Xk: Zeolitic imidazolate framework-8@polydopamine decorated carboxylated chitosan hydrogel with photocatalytic and photothermal antibacterial activity for infected wound healing. *J Colloid Interface Sci.* 2024;675:1040–51.
  63. Sun L, Zhang K, Wang J. Synergetic fabrication of ciprofloxacin-loaded ZIF-90 nanocarrier to enhance sustained pH-responsive delivery system for efficient bacterial inhibition in sepsis treatment: in vitro and in vivo evaluations. *Emergent Mater* 2024.
  64. Manna AC. Synthesis, Characterization, and Antimicrobial Activity of Zinc Oxide Nanoparticles. In: *Nano-Antimicrobials: Progress and Prospects*. Edited by Cioffi N, Rai M. Berlin, Heidelberg: Springer Berlin Heidelberg 2012:151–180.
  65. Yaqub A, Malkani N, Shabbir A, Ditta SA, Tanvir F, Ali S, Naz M, Kazmi SAR, Ullah R. Novel biosynthesis of copper nanoparticles using Zingiber and Allium sp. with synergic effect of doxycycline for Anticancer and Bactericidal Activity. *Curr Microbiol.* 2020;77(9):2287–99.
  66. Roy S, Hasan I, Guo B. Recent advances in nanoparticle-mediated antibacterial applications. *Coord Chem Rev.* 2023;482:215075.
  67. Walvekar P, Gannimani R, Govender T. Combination drug therapy via nanocarriers against infectious diseases. *Eur J Pharm Sci.* 2019;127:121–41.
  68. Naskar S, Kuotsu K, Sharma S. Chitosan-based nanoparticles as drug delivery systems: a review on two decades of research. *J Drug Target.* 2019;27(4):379–93.
  69. Moradialvand M, Asri N, Jahdkaran M, Beladi M, Hourri H. Advancements in nanoparticle-based strategies for enhanced antibacterial interventions. *Cell Biochem Biophys* 2024.
  70. Zhu G, Kang F, Tan Q, Li H, Zhang G, Wu M, Tan Y, Liu F-Q. Construction of copper-functionalized two-dimensional zeolitic imidazole framework-7 (ZIF-7) nanosheets for enhanced antibacterial and antibiofilm performance. *Prog Org Coat.* 2024;190:108383.
  71. Kermanshahi PK, Akhbari K. The antibacterial activity of three zeolitic-imidazolate frameworks and zinc oxide nanoparticles derived from them. *RSC Adv.* 2024;14(8):5601–8.
  72. Al-Awsi G, Alameri A, Al-Dhalimy A, Gabr G, Kianfar E. Application of nano-antibiotics in the diagnosis and treatment of infectious diseases. *Brazilian J Biology.* 2023;84:e264946.
  73. Wang Y, Zeng M, Fan T, Jia M, Yin R, Xue J, Xian L, Fan P, Zhan M. Biomimetic ZIF-8 nanoparticles: a Novel Approach for Biomimetic Drug Delivery systems. *Int J Nanomed.* 2024;19:5523–44.
  74. Chen X, Argandona SM, Melle F, Rampal N, Fairen-Jimenez D. Advances in surface functionalization of next-generation metal-organic frameworks for biomedical applications: design, strategies, and prospects. *Chem.* 2024;10(2):504–43.
  75. Ray Chowdhuri A, Tripathy S, Chandra S, Roy S, Sahu SK. A ZnO decorated chitosan–graphene oxide nanocomposite shows significantly enhanced antimicrobial activity with ROS generation. *RSC Adv.* 2015;5(61):49420–8.
  76. Sirelkhaitim A, Mahmud S, Seeni A, Kaus NHM, Ann LC, Bakhori SKM, Hasan H, Mohamad D. Review on Zinc Oxide nanoparticles: antibacterial activity and toxicity mechanism. *Nano-Micro Lett.* 2015;7(3):219–42.
  77. Srivastava P, Kim Y, Cho H, Kim K-s. Synergistic action between copper oxide (CuO) nanoparticles and anthraquinone-2-Carboxylic acid (AQ) against *Staphylococcus aureus*. In: *J Compos Sci* 2023;7.
  78. Kalaba MH, El-Sherbiny GM, Ewais EA, Darwesh OM, Moghannem SA. Green synthesis of zinc oxide nanoparticles (ZnO-NPs) by *Streptomyces baarnensis* and its active metabolite (Ka): a promising combination against multidrug-resistant ESKAPE pathogens and cytotoxicity. *BMC Microbiol.* 2024;24(1):254.
  79. Gautam A, Dabral H, Singh A, Tyagi S, Tyagi N, Srivastava D, Kushwaha HR, Singh A. Graphene-based metal/metal oxide nanocomposites as potential antibacterial agents: a mini-review. *Biomaterials Sci.* 2024;12(18):4630–49.

80. He J, Qu W, Feng Y, Jiang J, Luo J, Wu Y, Peng L. Multiple synergistic antibacterial melamine-impregnated paper based on nano Ag-doped ZIF-8. *Chem Eng J*. 2024;493:152453.
81. Barsola B, Saklani S, Pathania D, Kumari P, Sonu S, Rustagi S, Singh P, Raizada P, Moon TS, Kaushik A, et al. Exploring bio-nanomaterials as antibiotic allies to combat antimicrobial resistance. *Biofabrication*. 2024;16(4):042007.
82. Rai M, Ingle AP, Birla S, Yadav A, Santos CAD. Strategic role of selected noble metal nanoparticles in medicine. *Crit Rev Microbiol*. 2016;42(5):696–719.
83. Baptista PV, McCusker MP, Carvalho A, Ferreira DA, Mohan NM, Martins M, Fernandes AR. Nano-Strategies to fight Multidrug resistant Bacteria—A battle of the titans. *Front Microbiol* 2018;9.

### **Publisher's note**

Springer Nature remains neutral with regard to jurisdictional claims in published maps and institutional affiliations.